Highly stable and reversible lithium storage in SnO2 nanowires surface coated with a uniform hollow shell by atomic layer deposition

Guan, Cao; Wang, Xinghui; Zhang, Qing; Fan, Zhanxi; Zhang, Hua; Fan, Hong Jin

2014

Guan, C., Wang, X., Zhang, Q., Fan, Z., Zhang, H., & Fan, H. J. (2014). Highly stable and reversible lithium storage in SnO2 nanowires surface coated with a uniform hollow shell by atomic layer deposition. Nano letters, 14(8), 4852-4858.

https://hdl.handle.net/10356/99784

https://doi.org/10.1021/nl502192p

Highly Stable and Reversible Lithium Storage in SnO_2 Nanowires Surface Coated With A Uniform Hollow Shell by Atomic Layer Deposition

Cao Guan,[† §] **Xinghui Wang**,[‡] **Qing Zhang**,[‡] **Zhanxi Fan**,[&] **Hua Zhang**,[&] **and Hong Jin Fan**[†*]

[†] *School of Physical and Mathematical Sciences, Nanyang Technological University, 637371, Singapore*

[‡] *NOVITAS, Nanoelectronics Centre of Excellence, School of Electrical and Electronic Engineering, Nanyang Technological University, 639798, Singapore*

[&] *School of Materials Science and Engineering, Nanyang Technological University, 639798, Singapore*

[§] *Current Address: Department of Materials Science and Engineering, National University of Singapore, 117574 Singapore.*

* Address correspondence to fanhj@ntu.edu.sg

Abstract:

SnO_2 nanowires directly grown on flexible substrates can be a good electrode for lithium ion battery. However, Sn-based (metal Sn or SnO_2) anode materials always suffer from poor stability due to a large volume expansion during cycling. In this work, we utilize atomic layer deposition (ALD) to surface engineer SnO_2 nanowires, resulting in a new type of hollowed SnO_2-in-TiO_2 wire-in-tube nanostructure. This structure has radically improved rate capability and cycling stability than both bare SnO_2 nanowire and solid SnO_2@TiO_2 core-shell nanowire electrodes. Typically a relatively stable capacity of 393.3 mAh/g has been achieved after 1000 charge-discharge cycles at a current density of 400 mA/g, and 241.2 mAh/g at 3200 mA/g. It is believed that the uniform hollow TiO_2 shell provides a stable surface protection and the appropriate-sized gap effectively accommodates the expansion of the interior SnO_2 nanowire. This ALD-enabled method should be general to many other battery anode and cathode materials, providing a new and highly reproducible and controllable technique for improving battery performance.

Keywords: lithium-ion battery, tin oxide, nanowire, atomic layer deposition, battery anode

Lithium ion battery (LIB) has become the most widely commercialized energy storage device since more than 20 years ago.[1-3] However, the increasing demands in portable electronics and the future green transportation are pushing the research to new LIBs with higher energy density and longer cycling life. In terms of anode materials, so far the widely used graphite shows a limited theoretic capacity of 372 mAh/g, which is the bottleneck for the achievement of high energy densities. Metal oxides have been considered as good alternative candidates for LIB anodes, as they generally have much higher capacities than graphite and improved safety.[4-7]

Alloyed anodes, typically Sn based materials (such as SnO_2 and Sn) have been extensively studied for lithium storage, because they have high capacities and appropriate low onset potentials.[8, 9] However, during the charge-discharge process, these Sn-based anodes undergo severe pulverization with a huge volume expansion and continuous formation of solid-electrolyte interphase (SEI) layers. Therefore, these alloyed anodes usually have a very limited cycling ability.[9] To pave way for the commercial application of Sn based materials for LIB anodes, these issues should be carefully tackled in order to achieve improved cycling performance.

Several effective strategies have been carried out to improve the performance of Sn-based anodes. One way is to fabricate low dimensional nanostructures to ensure better structure stability than that of bulk materials, for example, SnO_2 nanowires, nanoflakes and 3D matrix have been reported with better mechanical stability and electrochemical properties.[10-14] Another way is to build an active or inactive matrix for Sn-based materials to buffer the volume change and simultaneously provide a conductive channel.[14-16, 18-22] For example, Co-Sn-C system has been demonstrated to be a good composite with high stability for high energy anodes,[23, 24] and a graphene/SnO_2/TiO_2 composite has shown highly reversible capacity[25]. Furthermore, efforts have also been carried out to build in hollow structures for Sn based materials, usually with other materials (such as carbon and TiO_2) as surface coating to stabilize SEI and accommodate the free expansion for Sn materials with the hollow space.[26-28] For example, a double shelled SnO_2/TiO_2 has shown better cycling and rate property than SnO_2 tube alone,[29] and another hollowed SnO_2 nanoplates with conformal carbon coating has demonstrated higher capacity and cycling ability than its single component.[30] Despite these efforts, the cycle stability is still not satisfactory enough and there is rare demonstration on such surface-engineered SnO_2 nanowires directly on flexible current collectors.

Herein, we report a novel hollowed wire-in-tube nanostructure of SnO_2-in-TiO_2 (SnO_2ΘTiO_2) on carbon cloth as an effective anode material for flexible LIBs. SnO_2 nanowires synthesized by vapor transport and deposition method have been demonstrated as a promising 1D structure with efficient electron transport, large interfacial area and high capacity.[31-33] We coat the single-crystalline SnO_2 nanowires with a hollow and conformal TiO_2 shell by using atomic layer deposition (ALD). The TiO_2 nanotube is electrochemical stable and has been reported as both durable anodes and effective surface coating material with volume expansion even less than that of graphite.[34, 35] The gap between the SnO_2 core and TiO_2 shell is designed to allow a nearly free expansion of the SnO_2 nanowire without severe pulverization and thus improve the cycling ability and rate capability. Optimization of the gap thickness and TiO_2 shell thickness towards superior performance is realized by ALD with great convenience.

With the wire-in-tube design, the nanowire electrode show a capacity and cycling ability that are among the best results of SnO_2 based metal oxides composites. A capacity of 883.1 mAh/g (2^{nd} cycle) at a current density of 400 mA/g is achieved, and the electrodes can be cycled with stable capacities of 494.9 and 393.3 mAh/g to 500 and 1000 cycles, respectively. In addition, the high active mass loading (~4.15 mg/cm^2) and the flexibility make this electrode promising for high-energy portable electronics. The work has also successfully demonstrated the application of ALD for flexible high performance energy storage devices.

Results and Discussion Figure 1a shows the SEM image of the carbon cloth after vapor deposition of SnO_2 nanowires, from which one can see the SnO_2 covers the whole surface of the carbon cloth (indicated by the white surface). Inset of Figure 1a shows the flexible nature of carbon cloth, which has received numerous attentions for flexible devices recently.[36-39] Figure 1b shows an enlarged SEM image of a typical part of carbon cloth after the SnO_2 growth, where the SnO_2 nanowires are randomly grown on the carbon cloth and have a length of more than 10 μm. Further enlarged SEM and TEM images of the SnO_2 nanowires are illustrated in Figure 1c-e. One can see that most of the nanowires have diameters in the range of 80-100 nm, which is in good agreement with previous reports.[21, 32, 40] The SnO_2 nanowires are densely grown on the carbon cloth fibers with a high mass loading of ~3 mg/cm^2. The SnO_2 nanowires on carbon cloth are also confirmed by XRD characterization (black curve in Figure 1f). Comparing with the red curve of pure carbon cloth, the peaks of the black curve can be well indexed to the rutile phase of SnO_2 (JCPDS, card no. 41-1445).

The SnO_2 nanowires were further surface engineered to improve its lithium-storage performance. In the following step, ZnO and TiO_2 thin shells were conformal coated using ALD, followed by removal of the ZnO middle layer in HCl, plus post annealing in Ar ambient. A hollowed SnO_2ΘTiO$_2$ wire-in-tube structure is thus formed. Figure 2a-c shows three typical SEM images of the SnO_2ΘTiO$_2$ from different parts of carbon cloth. One can see that after the above treatment the 1-D wire structure is fully preserved except for a larger and uniform diameter. The hollow core-shell structure and the gap can be clearly distinguished from the SEM images. As both wire core and tube shell are one-dimensional, it is easy to form line-to-line contact between them (see also below), which is essential for the good electrochemical performance.[41] Furthermore, we can also clearly see the hollowed wire-in-tube structures from the end of the wires (indicated by arrows in Figure 2b-c).

TEM investigation has also been carried out for better visualization of the hollowed SnO_2ΘTiO$_2$ core-shell nanostructure. One can see from the TEM images in Figure 2d-f that, the wire core, gap and tube shell can be clearly distinguished, and the gap and the shell are very uniform in the thickness, which is contributed from the layer-by-layer characteristics of ALD. The composition of SnO_2 and TiO_2 are further confirmed by HAADF-STEM image and corresponding STEM elemental mappings results (Figure 2g-j). From the mapping result, we can clearly distinguish the uniformly distributed SnO_2 and TiO_2, and the HRTEM images were also recorded and confirm the polycrystalline nature of the ALD TiO_2 shell.

To highlight, for this structure engineering of long nanowire electrode, the gap and the shell thicknesses can be easily controlled using different ALD cycles. Other shell materials can also be chosen for the shell for different applications, such as Li-S battery and electrocatalysts for oxygen reduction reactions. In this work, we choose 10 nm as the thickness for TiO_2 shell, based on the consideration that the surface coating should not be too thick to account for large mass ratio; also previous reports from our group demonstrated that 10 nm TiO_2 nanotubes are robust in LIB tests.[13, 42] As for the gap thickness, we choose ~45 nm by considering the 300% volume expansion of SnO_2 nanowires[43] (Detailed calculation is presented in supporting information). In order to highlight the advantage of the hollow structure in LIB properties, solid core-shell structure of SnO_2@TiO_2 with no gap has also been fabricated and studied (SEM and TEM images are shown in supporting information, Figure S1).

All the three materials, bare SnO_2, solid core-shell SnO_2@TiO_2, and hollowed wire-in-tube SnO_2ΘTiO_2 have been studied in the following electrochemical tests. The CV curves are shown in Figure S2a-c. All the CV curves show a big cathodic peak at ~0.3 V during the first discharge, which is caused by the formation of Li_2O (i.e., activation of SnO_2) and the SEI film.[44] In the second and third cycles, the reduction peaks of SnO_2 to Sn and subsequently Sn to Li_xSn can be clearly observed at ~0.8 and ~0.2 V, respectively. The detailed reactions are as follows.[29, 32]

$$SnO_2 + 4Li^+ + 4e^- \rightarrow Sn + 2Li_2O \quad (1)$$

$$xLi^+ + xe^- + Sn \leftrightarrow Li_xSn \ (0 \le x \le 4.4). \quad (2)$$

During the charge process, two peaks located at ~0.6 V and 1.3 V are related to de-alloy of Li_xSn and the subsequent oxidation of metallic Sn^0 particles.[16, 45, 46] No obvious peaks of the reaction for TiO_2 is observed in the range of ~1.5–2 V; this absence could be due to rather low mass percentage and capacity of TiO_2.

The galvanostatic charge-discharge curves of the three materials are shown in Figure S2d-f. The materials are first discharged from open circuit potential to 0.005 V at a current density of 400 mA/g, during which a large amount of capacity is lost following the formation of SEI layer, reduction of SnO_2 to Li_xSn, as well as a possible formation of a conductive $Li_yTi_{1-y}O_2$ phase with the reduction of TiO_2.[25, 37] During the following charge-discharge process, the voltage range is fixed to be 0.005–1.5 V, thus the $Li_yTi_{1-y}O_2$ will not be oxidized again but served as a conductive protection.[47] The initial discharge capacity of the SnO_2, SnO_2@TiO_2 and SnO_2ΘTiO_2 are 2049.9, 1658.5, and 1421.3 mAh/g, respectively. The corresponding columbic efficiencies (CE) are 45.2%, 57.9%, and 67.7%. The poor CEs of SnO_2-based electrodes are mainly due to the formation of SEI and the irreversible reduction between SnO_2 and Sn.[29] The increased CE of the hollowed core-shell nanowire electrode could be related to the TiO_2 coating, which confines the formation of Li_2O and SEI directly on SnO_2 during the first discharge and also prevent the loss of active material.

The hollowed TiO_2 shell improves both the cyclic stability and rate capability. Figure 3a depicts the cycling curves for the three types of electrodes at the same current of 400 mA/g. For the bare SnO_2 nanowire, a starting capacity can last only for the first 20 cycles of charge-discharge, and drops sharply to nearly zero after 100 cycles. Such a poor cycling stability of the

bare SnO_2 is not surprising to consider the 300% volume expansion and the continuously formed SEI layer that isolates the active materials. These are the common problems for alloyed anodes.[9, 25, 48-51] For the solid core-shell SnO_2@TiO_2 structure, the capacity can be stabilized for the first 35 cycles, which is slightly better than the bare SnO_2 due to the more stable TiO_2 coating layer. However, its capacity still drops fast afterwards with a remaining capacity of only ~218 mAh/g after 200 cycles. This unstable cycling durability of the solid core-shell structure can be attributed to the fracture of the outer TiO_2 layer induced by the inner stress from the huge volume expansion[43]. To achieve a better cycling ability, a proper hollowed space to buffer the volume expansion is thus beneficial. As demonstrated in Figure 3a, a significantly improved cycling ability is achieved for the hollowed wire-in-tube structure of SnO_2ΘTiO_2 electrode, which is able to maintain a capacity of 494.9 mAh/g after 500 cycles. Further test shows a capacity of 393.3 mAh/g can be achieved up to 1000 cycles. The cycling stability is better than many previously reported SnO_2-metal oxide composites, such as SnO_2@TiO_2 double-shell nanotubes,[29] Fe_2O_3/SnO_2 nano-heterostructure,[40] and SnO_2-MnO_2-SnO_2 sandwich-structured nanotubes.[52] As discussed previously, the gap between the SnO_2 nanowire and TiO_2 shell is able to buffer the volume expansion, and also prevents the formation of SEI layer directly on the SnO_2 nanowires. During the long-time cycling, the columbic efficiency for the SnO_2ΘTiO_2 is mostly above 99% (except for the first few cycles), showing its good electrochemical reversibility (Figure 3b). Due to the high mass loading of the active materials, the initial areal capacity of the SnO_2ΘTiO_2 is 5.90 mAh/cm^2, and it maintains 1.63 mAh/cm^2 after 1000 cycles, which is much larger than the areal capacities achieved by other Sn/metal oxide composites (such as TiO_2/SnO, α-Fe_2O_3/SnO_2, SnO_2/Fe_2O_3),[40, 53, 54] and other alloy-anode based composites (such as Si/void/C, and SnO_2@Si).[32, 41] One thing to notice is that the carbon cloth has a low capacity of ~55 mAh/g and its contribution would be even less when covered with a thick layer of active materials[55] (e.g. in present work the carbon cloth has a capacity of ~18 mAh/g after 200 cycles). In addition, the partially reversible SEI can also contribute to an extra capacity. These two factors may account for the measured overall capacities higher than their theoretical ones.[56] In order for a fair comparison to literature, we hereby include the mass of active materials only (SnO_2 and TiO_2) for the calculation of capacity. Even if we take into account the mass of carbon cloth, the whole electrode (active material mass ratio is ~29.3%) can still deliver a capacity of

416.8 mAh/g. The capacity contribution by the carbon cloth is estimated to be less than 9.0% (see detailed estimation in Supporting Information).

The sheath of the SnO_2 nanowires by the ~10 nm thick TiO_2 film does not sacrifice the kinetics. The rate capability results of the three types of nanowire electrodes are shown in Figure 3c. Although the SnO_2ΘTiO_2 shows a lower capacity than the other two electrodes in the first few cycles, it maintains an evidently better stability afterwards so to provide a higher capacity at high rates. When the current density increases to 3200 mA/g, the wire-in-tube structure can still maintain a capacity of 241.2 mAh/g, while the capacities of the solid core-shell nanowire and bare SnO_2 nanowire electrodes are only 147.3 and 109.3 mAh/g, respectively. More importantly, when the current returns to 200 mA/g, the wire-in-tube structure illustrates a capacity of 804.1 mAh/g, which nearly fully recovers the capacity during the 2^{nd} cycle (826.0 mAh/g), indicating its excellent reaction reversibility. In addition, the wire-in-tube structure was further tested by varying the current densities for another 70 cycles, and then charge-discharged for another 120 cycles. The stable capacity retention during the long-cycle test is a clear manifestation of its excellent rate capability and cycling stability of the hollowed core-shell nanowire electrodes. In contrast, for the bare SnO_2 and solid core-shell SnO_2@TiO_2 electrodes, their abilities for high-rate capacity retention and reaction reversibility are both very poor.

To further verify the high durability of the wire-in-tube structure, the microstructure of the wire-in-tube electrode after long-time cycling is examined by both SEM and TEM. As shown in Figure 4a, one can see the 1-D morphology of the wires is well preserved after 600 cycles of charge-discharge, and the clear wire-in-tube structure can be still resolved. In contrast, the solid core-shell structure (SnO_2@TiO_2) after 200 cycles shows severe damage and fracture (Figure 4b). Additional large-scale SEM images are shown in Figure S3. TEM images were also recorded from the SnO_2ΘTiO_2 nanowires after the electrode was cycled 600 times. One can see from Figure 4c-d that, after repeated cycling, the inner SnO_2 nanowire fractures but is still confined within the TiO_2 shell, leaving the overall core-shell structure preserved.

The optimized gap thickness of 45 nm is verified by comparing the cyclic stabilities to another two control samples with ~20 and ~60 nm gap thicknesses (TiO_2 shell thickness kept the same, 10 nm). Figure S4 show that the nanowire electrodes with three different gap thicknesses have roughly the same capacity, but the 45 nm one exhibit the best stability. Nonetheless, the 45 nm gap thickness is based on an average thickness of the SnO_2 nanowires. That may explain the non-

negligible degradation of the capacity over repeated charge-discharges, and the observation of cracks for some wires. Other nanowire diameters will correspond to a different gap thickness according to the estimation (Supporting Information).

To wrap up, the schematic illustration of the three types of nanowire structure (bare SnO_2, SnO_2@TiO_2 and SnO_2ΘTiO_2) is shown in Figure 5. A bare SnO_2 nanowire will undergo a huge volume expansion and fracture during cycling, resulting in a fast structural deterioration of the long nanowires and thus a very poor cycling stability. Proper coating of protective layer directly on the surface (TiO_2 in this case) will effectively stabilize the SEI, but the solid core-shell is still prone to damage due to the SnO_2 expansion stress during the cycling, as illustrated in Figure 5d and also confirmed by SEM image (Figure 4b). With a rationally designed hollow space between the SnO_2 core and TiO_2 shell (Figure 5a-c), the volume expansion of SnO_2 can be effectively accommodated so that the stress on the outer TiO_2 layer and the SEI layer can be released. In this way, the wire-in-tube structure of SnO_2ΘTiO_2 can be very stable. In addition, because of the 1-D structure, it is easy to have a line-to-line contact between the core and shell, which can ensure improved electric contact and ion/electron transfer compared with point-to-point contact in powder electrodes.[41, 57] Finally, the precise control in thickness of both the gap and shell layer makes this method widely applicable for other electrodes materials with a large volume expansion ratio (including Si).

In conclusion, a hollowed wire-in-tube structure of SnO_2ΘTiO_2 on carbon cloth with a high mass loading (~4.15 mg/cm^2) has been fabricated by vapor deposition followed with structure engineering by ALD. When tested as flexible anode for lithium ion battery, the wire-in-tube structure has demonstrated improved cycling stability and high-rate capacities, compared with the bare core or solid core-shell structure. The outstanding Li storage performance of SnO_2ΘTiO_2 can be attributed to the middle gap design and uniform surface thin sheath, which can simultaneously stabilize SEI and accommodate volume expansion of the SnO_2 core wire. Our ALD assisted structure engineering can be applied to many other electrode materials and thus find potential applications for flexible high-energy storage devices.

Experimental

Material synthesis. (1) SnO_2 nanowires were obtained by vapor deposition method using Sn powder as source, sputter-coated Au as vapor-liquid-solid catalyst, and carbon cloth (2×3 cm^2) as substrates. The growth was conducted with temperature ramped to 850 °C at a rate of 50 °C /min

and kept for 1 h under a constant argon (with 0.5% oxygen) flow (50 sccm) and pressure (1 mbar). (2) ALD coating of ZnO and TiO_2 on the carbon cloth with SnO_2 nanowires was carried out using a Beneq system (TFS 200) at 200˚C and 120 ˚C, respectively.[58] Diethyl zinc (DEZ), $TiCl_4$ and water were used as the zinc, titanium and oxygen source, respectively. During the deposition, the reaction chamber was maintained at 1.0 mbar with a steady N_2 steam at 200 SCCM (cubic centimeter per minute). Each ALD cycle consisted of a 300-ms precursor pulse and 2-s purging time with N_2. (3) The samples were further immersed in a 0.1 M HCl solution in order to dissolve the ZnO sacrificial layer, followed by washing and annealing in Ar at 400 ˚C for 2 h.

Characterization. Samples were characterized by scanning electron microscopy (SEM, JSM-6700F, 5.0-10.0 kV), transmission electron microscopy (TEM, JEM-2010FEF, 200 kV), and powder X-ray diffraction (XRD, Bruker D-8 Avance). The mass of electrode materials was measured on an AX/MX/UMX Balance (METTLER TOLEDO, maximum=5.1 g; delta = 0.001 mg).

Electrochemical test. Electrochemical measurements were performed using two-electrode CR2032 (3 V) coin-type cells with lithium foil serving as both counter and reference electrodes under ambient temperature. Active material on carbon cloth (1×1 cm^2) was used directly as working electrode. The electrolyte was 1 M $LiPF_6$ in a 50: 50 (w/w) mixture of ethylene carbonate (EC) and dimethyl carbonate (DMC). Cell assembly was carried out in an argon-filled glove box with both moisture and oxygen contents below 1.0 ppm. Electrochemical tests were performed using a NEWARE battery tester. The discharge of the first cycle is performed from open circuit potential to 0.005V, and all the following tests were carried out at a voltage window of 0.005–1.5 V. Cyclic voltammetry (CV, 0.005–3 V, 0.5 mV s^{-1}) was performed using an electrochemical workstation (CHI 760D).

Conflict of Interests: The authors declare no competing financial interests.

Supporting Information Available: SEM-TEM images of solid core-shell structure of SnO_2@TiO_2, detailed CV and charge-discharge curves, SEM images of the solid and hollowed core-shell nanowires after cycles, TEM images and stability tests of hollow core-shell nanowires of different gap thicknesses. This material is available free of charge via the Internet at http://pubs.acs.org.

Acknowledgements. This research is funded by SERC Public Sector Research Funding (Grant number 1121202012), Agency for Science, Technology, and Research (A*STAR), and partly by the joint Singaporean-German Research Projects (SGP-PROG-021). H.Z. thanks the supported from MOE under AcRF Tier 2 (ARC 26/13, No. MOE2013-T2-1-034), AcRF Tier 1 (RG 61/12, RGT18/13 and RG5/13), and Start-Up Grant (M4080865.070) in Singapore. This Research is also conducted by NTU-HUJ-BGU Nanomaterials for Energy and Water Management Programme under the Campus for Research Excellence and Technological Enterprise (CREATE), that is supported by the National Research Foundation, Prime Minister's Office, Singapore.

REFERENCES AND NOTES

1. Idota, Y.; Kubota, T.; Matsufuji, A.; Maekawa, Y.; Miyasaka, T. *Science* **1997,** 276, 1395-1397.
2. Magasinski, A.; Dixon, P.; Hertzberg, B.; Kvit, A.; Ayala, J.; Yushin, G. *Nat. Mater.* **2010,** 9, 353-358.
3. Meng, X.; Yang, X.-Q.; Sun, X. *Adv. Mater.* **2012,** 24, 3589-3615.
4. Jiang, C.; Hosono, E.; Zhou, H. *Nano Today* **2006,** 1, 28-33.
5. Wang, X.; Li, X.; Sun, X.; Li, F.; Liu, Q.; Wang, Q.; He, D. *J. Mater. Chem.* **2011,** 21, 3571-3573.
6. Jiang, J.; Li, Y.; Liu, J.; Huang, X.; Yuan, C.; Lou, X. W. *Adv. Mater.* **2012,** 24, 5166-5180.
7. Wei, W.; Wang, Z.; Liu, Z.; Liu, Y.; He, L.; Chen, D.; Umar, A.; Guo, L.; Li, J. *J. Power Sources* **2013,** 238, 376-387.
8. Huang, J. Y.; Zhong, L.; Wang, C. M.; Sullivan, J. P.; Xu, W.; Zhang, L. Q.; Mao, S. X.; Hudak, N. S.; Liu, X. H.; Subramanian, A.; Fan, H.; Qi, L.; Kushima, A.; Li, J. *Science* **2010,** 330, 1515-1520.
9. Wang, B.; Luo, B.; Li, X.; Zhi, L. *Mater. Today* **2012,** 15, 544-552.
10. Liang, Y.; Fang, B. *Mater. Res. Bull.* **2013,** 48, 4118-4124.
11. Liu, J.; Li, Y.; Huang, X.; Ding, R.; Hu, Y.; Jiang, J.; Liao, L. *J. Mater. Chem.* **2009,** 19, 1859-1864.
12. Haag, J. M.; Pattanaik, G.; Durstock, M. F. *Adv. Mater.* **2013,** 25, 3238-3243.
13. Zhu, C.; Xia, X.; Liu, J.; Fan, Z.; Chao, D.; Zhang, H.; Fan, H. J. *Nano Energy* **2014,** 4, 105-112.
14. Park, M.-S.; Wang, G.-X.; Kang, Y.-M.; Wexler, D.; Dou, S.-X.; Liu, H.-K. *Angew. Chem. Int. Ed.* **2007,** 119, 764-767.
15. Derrien, G.; Hassoun, J.; Panero, S.; Scrosati, B. *Adv. Mater.* **2007,** 19, 2336-2340.
16. Lin, J.; Peng, Z.; Xiang, C.; Ruan, G.; Yan, Z.; Natelson, D.; Tour, J. M. *ACS Nano* **2013,** 7, 6001-6006.
17. Luo, B.; Wang, B.; Li, X.; Jia, Y.; Liang, M.; Zhi, L. *Adv. Mater.* **2012,** 24, 3538-3543.
18. Shin, H. C.; Liu, M. *Adv. Funct. Mater.* **2005,** 15, 582-586.
19. Xu, Y.; Liu, Q.; Zhu, Y.; Liu, Y.; Langrock, A.; Zachariah, M. R.; Wang, C. *Nano Lett.* **2013,** 13, 470-474.
20. Yu, Y.; Gu, L.; Zhu, C.; van Aken, P. A.; Maier, J. *J. Am. Chem. Soc.* **2009,** 131, 15984-15985.
21. Kim, D.-W.; Hwang, I.-S.; Kwon, S. J.; Kang, H.-Y.; Park, K.-S.; Choi, Y.-J.; Choi, K.-J.; Park, J.-G. *Nano Lett.* **2007,** 7, 3041-3045.
22. Li, X.; Dhanabalan, A.; Gu, L.; Wang, C. *Adv. Energy Mater.* **2012,** 2, 238-244.
23. Hassoun, J.; Mulas, G.; Panero, S.; Scrosati, B. *Electrochem. Commun.* **2007,** 9, 2075-2081.
24. Cui, W.; Wang, F.; Wang, J.; Wang, C.; Xia, Y. *Electrochim. Acta* **2011,** 56, 4812-4818.

25. Tang, Y.; Wu, D.; Chen, S.; Zhang, F.; Jia, J.; Feng, X. *Energy & Environ. Sci.* **2013,** 6, 2447-2451.

26. Chen, Z.; Zhou, M.; Cao, Y.; Ai, X.; Yang, H.; Liu, J. *Adv. Energy Mater.* **2012,** 2, 95-102.

27. Ji, L.; Tan, Z.; Kuykendall, T.; An, E. J.; Fu, Y.; Battaglia, V.; Zhang, Y. *Energy & Environ. Sci.* **2011,** 4, 3611-3616.

28. Lai, X.; Halpert, J. E.; Wang, D. *Energy & Environ. Sci.* **2012,** 5, 5604-5618.

29. Jeun, J.-H.; Park, K.-Y.; Kim, D.-H.; Kim, W.-S.; Kim, H.-C.; Lee, B.-S.; Kim, H.; Yu, W.-R.; Kang, K.; Hong, S.-H. *Nanoscale* **2013,** 5, 8480-8483.

30. Zhang, L.; Zhang, G.; Wu, H. B.; Yu, L.; Lou, X. W. *Adv. Mater.* **2013,** 25, 2589-2593.

31. Ko, Y.-D.; Kang, J.-G.; Park, J.-G.; Lee, S.; Kim, D.-W. *Nanotechnology* **2009,** 20, 455701.

32. Ren, W.; Wang, C.; Lu, L.; Li, D.; Cheng, C.; Liu, J. *J. Mater. Chem. A* **2013,** 1, 13433-13438.

33. Zhou, W.; Tay, Y. Y.; Jia, X.; Yau Wai, D. Y.; Jiang, J.; Hoon, H. H.; Yu, T. *Nanoscale* **2012,** 4, 4459-4463.

34. Kim, M. S.; Lee, T.-W.; Park, J. H. *J. Electrochem. Soc.* **2009,** 156, A584-A588.

35. Lu, X.; Wang, G.; Zhai, T.; Yu, M.; Gan, J.; Tong, Y.; Li, Y. *Nano Lett.* **2012,** 12, 1690-1696.

36. Liu, B.; Zhang, J.; Wang, X.; Chen, G.; Chen, D.; Zhou, C.; Shen, G. *Nano Lett.* **2012,** 12, 3005-3011.

37. Zhang, X.; Gong, L.; Liu, K.; Cao, Y.; Xiao, X.; Sun, W.; Hu, X.; Gao, Y.; Chen, J.; Zhou, J.; Wang, Z. L. *Adv. Mater.* **2010,** 22, 5292-5296.

38. Zhou, G.; Li, F.; Cheng, H.-M. *Energy & Environ. Sci.* **2014,** 7, 1307-1338.

39. Han, X.; Xu, Y.; Chen, X.; Chen, Y.-C.; Weadock, N.; Wan, J.; Zhu, H.; Liu, Y.; Li, H.; Rubloff, G.; Wang, C.; Hu, L. *Nano Energy* **2013,** 2, 1197-1206.

40. Zhou, W.; Cheng, C.; Liu, J.; Tay, Y. Y.; Jiang, J.; Jia, X.; Zhang, J.; Gong, H.; Hng, H. H.; Yu, T.; Fan, H. J. *Adv. Funct. Mater.* **2011,** 21, 2439-2445.

41. Wang, B.; Li, X.; Zhang, X.; Luo, B.; Zhang, Y.; Zhi, L. *Adv. Mater.* **2013,** 25, 3560-3565.

42. Luo, J.; Xia, X.; Luo, Y.; Guan, C.; Liu, J.; Qi, X.; Ng, C. F.; Yu, T.; Zhang, H.; Fan, H. J. *Adv. Energy Mater.* **2013,** 3, 737-743.

43. Zhao, K.; Pharr, M.; Hartle, L.; Vlassak, J. J.; Suo, Z. *J. Power Sources* **2012,** 218, 6-14.

44. Xu, W.; Canfield, N. L.; Wang, D.; Xiao, J.; Nie, Z.; Zhang, J.-G. *J. Power Sources* **2010,** 195, 7403-7408.

45. Aravindan, V.; Jinesh, K. B.; Prabhakar, R. R.; Kale, V. S.; Madhavi, S. *Nano Energy* **2013,** 2, 720-725.

46. He, M.; Yuan, L.; Hu, X.; Zhang, W.; Shu, J.; Huang, Y. *Nanoscale* **2013,** 5, 3298-3305.

47. Ji, G.; Ding, B.; Ma, Y.; Lee, J. Y. *Energy Technology* **2013,** 1, 567-572.

48. Zhang, W.-J. *J. Power Sources* **2011,** 196, 13-24.

49. Xiao, Q.; Fan, Y.; Wang, X.; Susantyoko, R. A.; Zhang, Q. *Energy & Environ. Sci.* **2014,** 7, 655-661.

50. Liu, M.; Li, X.; Ming, H.; Adkins, J.; Zhao, X.; Su, L.; Zhou, Q.; Zheng, J. *New J. Chem.* **2013,** 37, 2096-2102.

51. Hassan, F. M.; Chabot, V.; Elsayed, A. R.; Xiao, X.; Chen, Z. *Nano Lett.* **2013,** 14, 277-283.

52. Xing, L.-L.; He, B.; Nie, Y.-X.; Deng, P.; Cui, C.-X.; Xue, X.-Y. *Mater. Lett.* **2013,** 105, 169-172.

53. Ortiz, G. F.; Hanzu, I.; Lavela, P.; Knauth, P.; Tirado, J. L.; Djenizian, T. *Chem. Mater.* **2010,** 22, 1926-1932.

54. Zeng, W.; Zheng, F.; Li, R.; Zhan, Y.; Li, Y.; Liu, J. *Nanoscale* **2012,** 4, 2760-2765.

55. Hou, X.; Wang, X.; Liu, B.; Wang, Q.; Wang, Z.; Chen, D.; Shen, G. *ChemElectroChem* **2014,** 1, 108-115.

56. Hu, Y.-Y.; Liu, Z.; Nam, K.-W.; Borkiewicz, O. J.; Cheng, J.; Hua, X.; Dunstan, M. T.; Yu, X.; Wiaderek, K. M.; Du, L.-S.; Chapman, K. W.; Chupas, P. J.; Yang, X.-Q.; Grey, C. P. *Nat. Mater.* **2013,** 12, 1130-1136.

57. Wu, H.; Zheng, G.; Liu, N.; Carney, T. J.; Yang, Y.; Cui, Y. *Nano Lett.* **2012,** 12, 904-909.

58. Guan, C.; Xia, X.; Meng, N.; Zeng, Z.; Cao, X.; Soci, C.; Zhang, H.; Fan, H. J. *Energy & Environ. Sci.* **2012,** 5, 9085-9090.

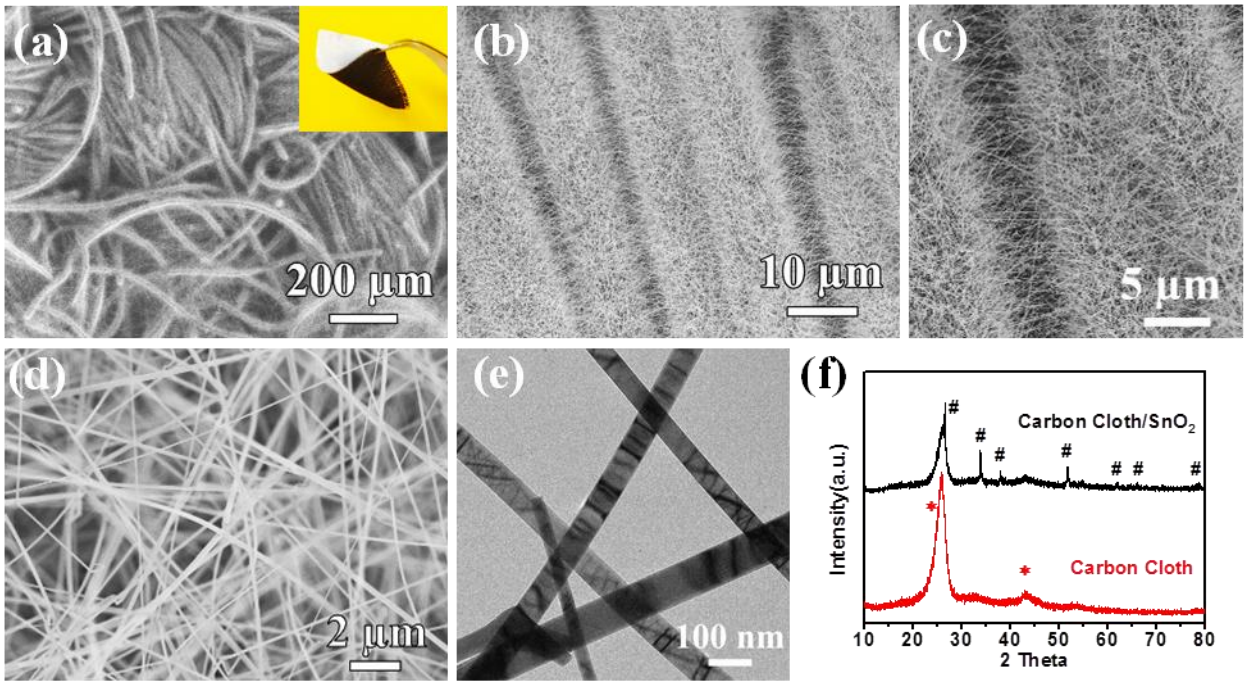

Figure 1. (a-d) SEM and (e) TEM images of the SnO_2 nanowires grown on carbon cloth. Insert in (a) shows a piece of flexible carbon cloth after SnO_2 growth on one side. (f) XRD patterns of the SnO_2 nanowires on carbon cloth and bare carbon cloth.

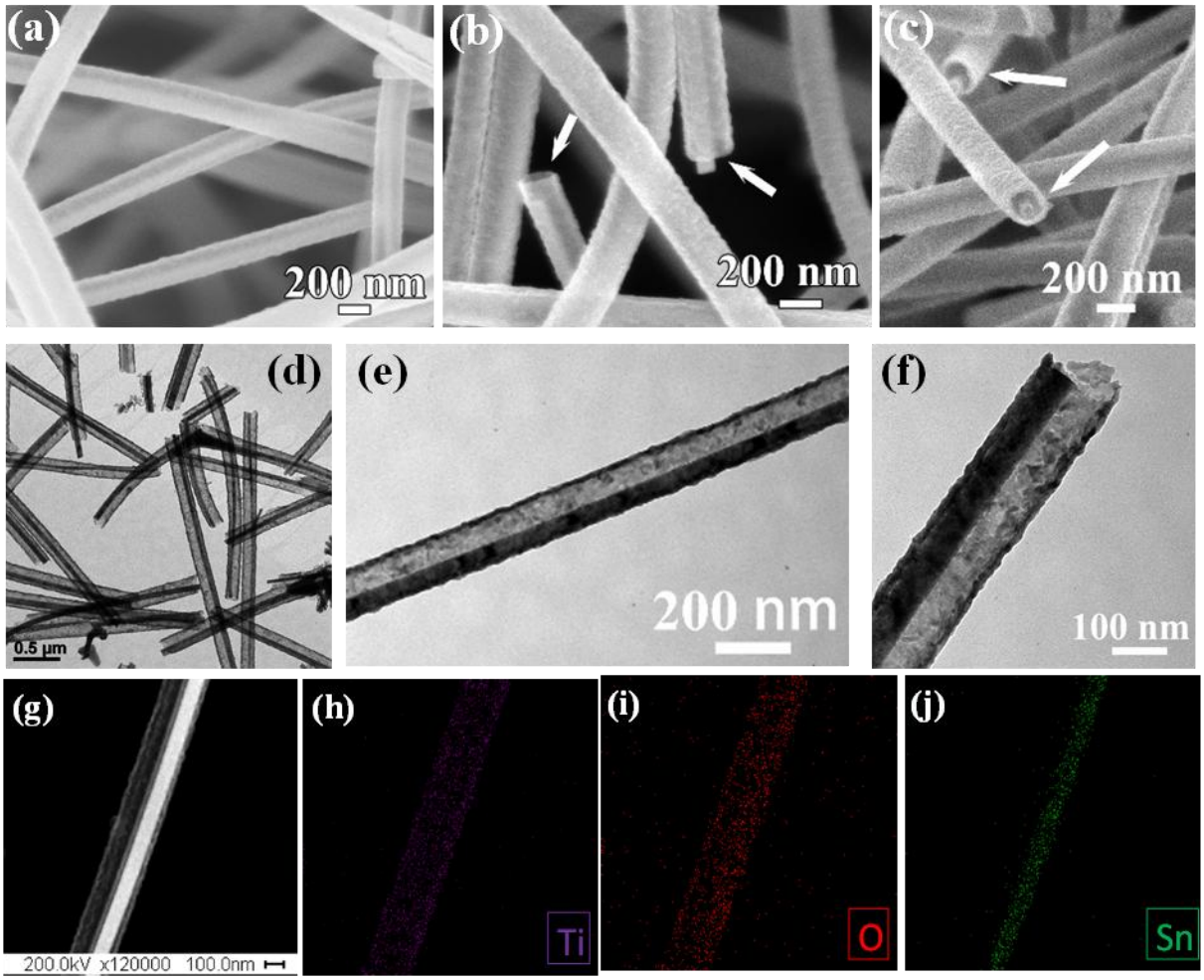

Figure 2. (a-c) SEM and (d-f) TEM images of the SnO_2ΘTiO_2 wire-in-tube nanostructure. The arrows indicate the tips of the nanowires showing clearly the inner wire core, gap and outer shell. (g) HAADF-STEM image of a single hollowed SnO_2@TiO_2 nanowire, and (h-j) the corresponding STEM element mapping results.

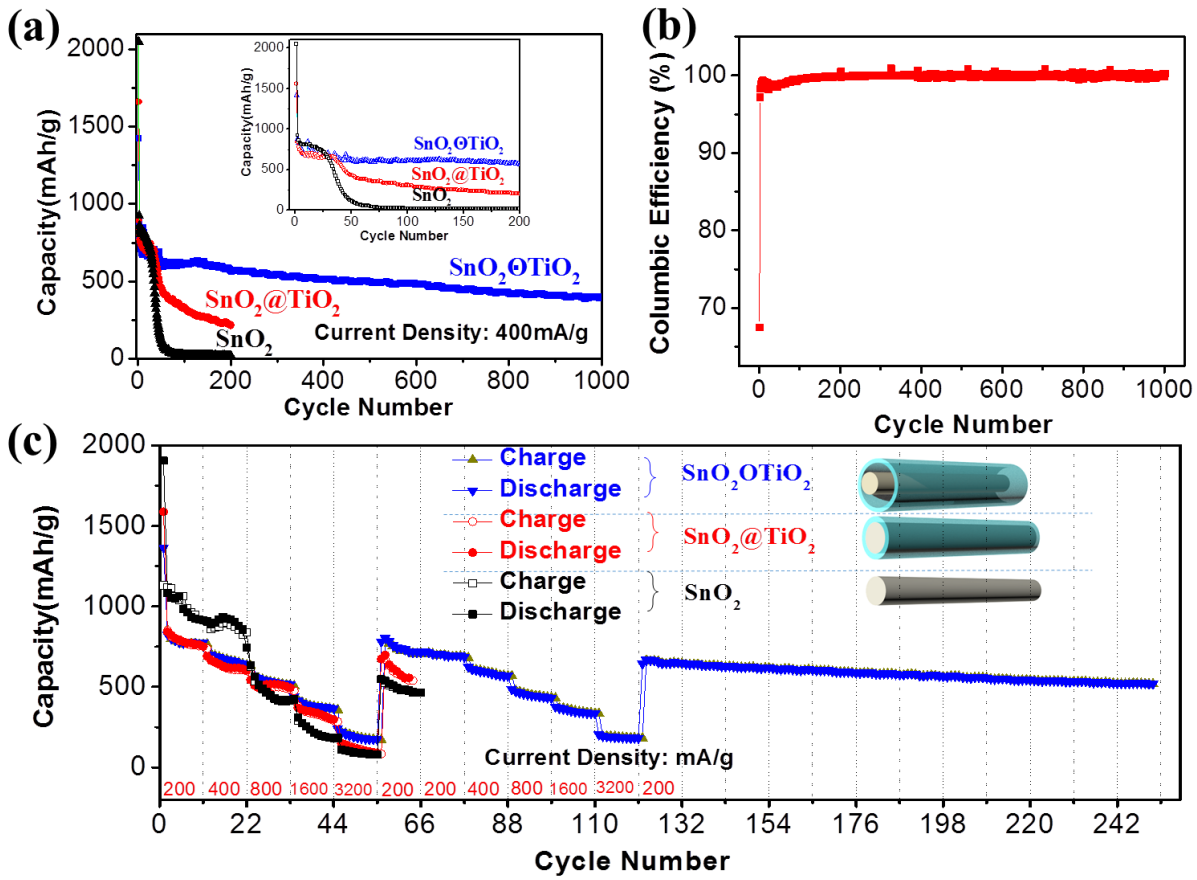

Figure 3. (a) Cycling stability test of the three electrodes: bare SnO_2 nanowires, SnO_2@TiO_2 solid core-shell nanowires, and SnO_2ΘTiO_2 wire-in-tube structure. Current density is 400 mA/g. Inset shows the first 200 cycles. (b) Columbic efficiency of SnO_2ΘTiO_2 electrode during the cycling. (c) Rate capability of the three electrodes (i.e., capacity at different current rates).

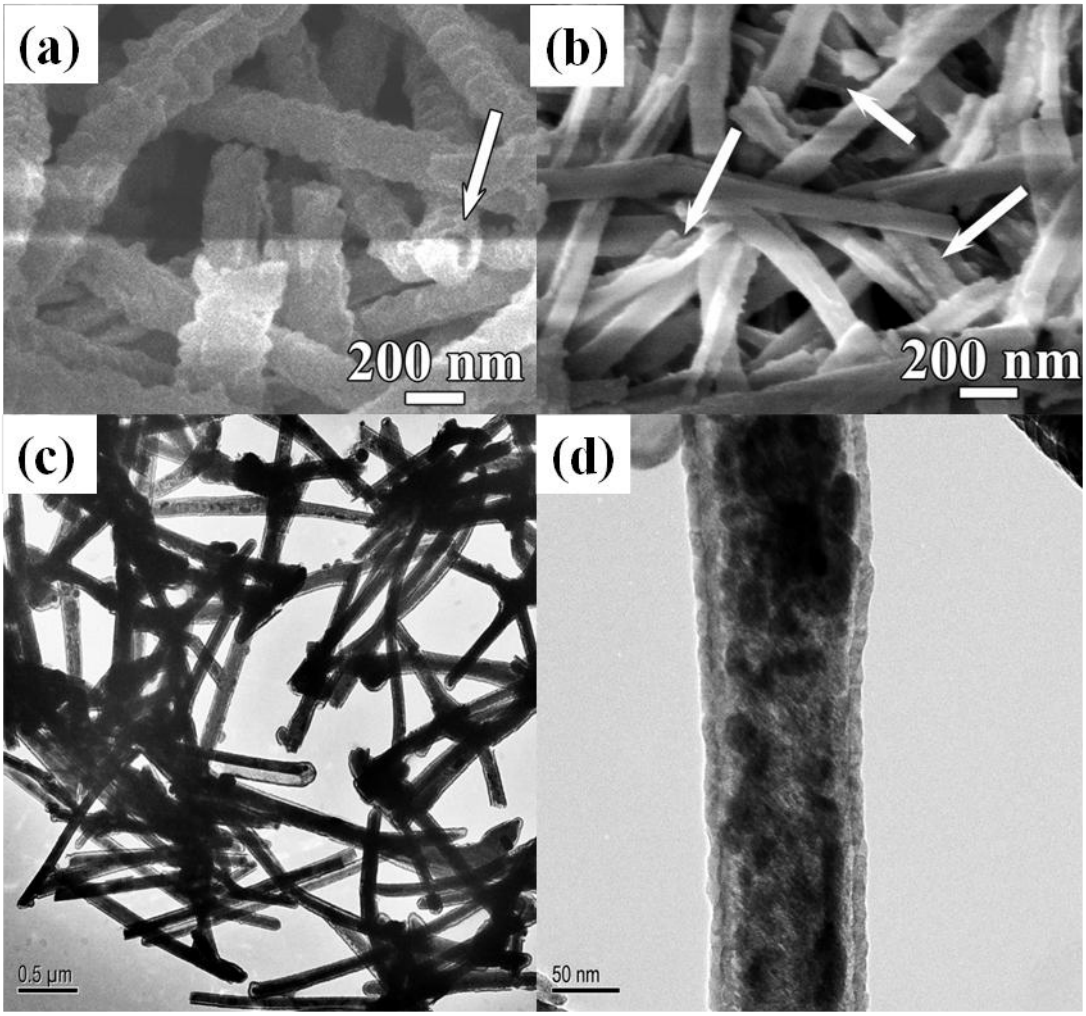

Figure 4. SEM images obtained from (a) SnO_2ΘTiO_2 and (b) SnO_2@TiO_2 after 600 and 200 charge-discharge cycles, respectively. (c-d) TEM images obtained from SnO_2ΘTiO_2 after 600 charge-discharge cycles. The expanded and amorphous SnO2 nanowire core after cycling is still refrained within the TiO_2 shell.

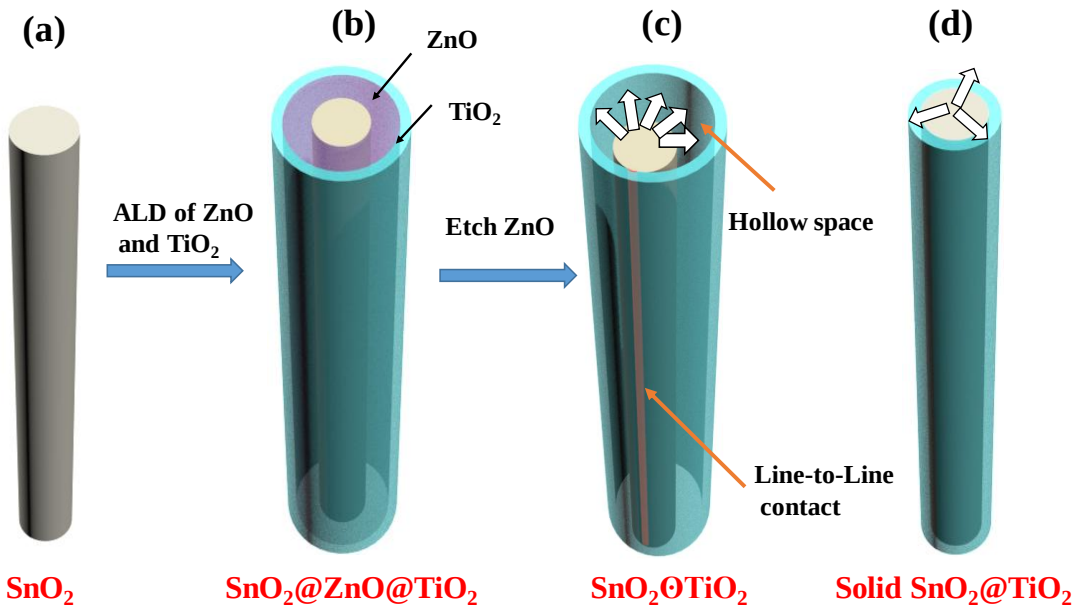

Figure 5. (a-c) Schematics of the fabrication process of the $SnO_2\Theta TiO_2$ wire-in-tube structure. (d) Solid core-shell nanowires for comparison. With an appropriate selection of the shell and gap thicknesses, the surface coating and hollow design can ensure line-to-line contact (marked by red line in c) for electrochemical reaction and accommodate volume expansion (marked by white arrows). In contrast, the solid core-shell nanowire structure has no space for free expansion, thus it tends to collapse during charge-discharge cycles.

TOC graph

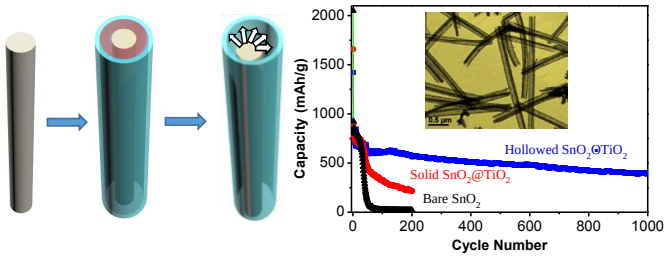
2000
1500
1000
500
0
Capacity (mAh/g)
0
200
400
600
800
1000
Cycle Number
Hollowed SnO2@TiO2
Solid SnO2@TiO2
Bare SnO2
0.5 μm